Through-wall imaging by TE and TM hybrid polarization inversion based on FDFD and frequency hopping scheme

Sun, Shilong

DOI
10.1049/cp.2015.1313

Publication date
2015

Document Version
Final published version

Published in
IET International Radar Conference 2015

Through-wall Imaging by TE and TM Hybrid Polarization Inversion Based on FDFD and Frequency Hopping Scheme

Shilong Sun*, Bert Jan Kooij*, Tian Jin*† and Alexander Yarovoy*
*Faculty Electrical Engineering, Mathematics and Computer Science
Delft University of Technology, Delft, 2628CD, The Netherlands
Email: S.Sun@tudelft.nl, B.J.Kooij@tudelft.nl, Tianjin@nudt.edu.cn, A.Yarovoy@tudelft.nl
†on leave from College of Electronic Science and Engineering
National University of Defense Technology, Changsha, 410073, China

***Keywords*—Contrast Source Inversion (CSI), FDFD, Through-wall Imaging (TWI), frequency hopping.**

***Abstract*—In this paper, TE and TM hybrid polarization contrast source inversion (CSI) based on FDFD and frequency hopping scheme is applied to through-wall imaging (TWI). The through-wall configuration is incorporated as a priori information in the background configuration of our FDFD inversion scheme. Multiple frequencies are used to improve the imaging performance. As the permittivity and conductivity of the targets are always higher than those of the air, the positivity of the contrast is utilized as a priori information to enhance the inversion performance. 2D simulation results show that the permittivity and conductivity of the targets behind the wall can be well reconstructed.**

I. Introduction

Inversion techniques have been applied extensively in the fields such as seismic imaging, medical imaging, radar imaging, and so forth. Basically, inversion methods can be divided into two families – time domain based methods and frequency domain based methods. One obvious advantage of the time domain methods is that it is able to utilize all the contribution from a wide range of frequency components. However, the inversion performance can be seriously degraded when dealing with the dispersive materials. Moreover, the system design of the time domain methods are much more complex than that of the frequency domain methods.

Among frequency domain inversion techniques, Contrast Source Inversion (CSI) method has been widely used since it was first proposed by van den Berg et al. [1]. Application of the method to the subsurface object detection in combination with integral equations based on the Electric Field Integral Equation (EFIE) formulation has been considered in [2]. In addition, Crocco et al. [3], [4], applied the so called contrast source-extended Born-model to 2D subsurface scattering problems. Later the CSI technique was introduced in combination with a Finite Difference Frequency Domain (FDFD) scheme by Abubakar et al. [5], [6]. The scheme based on the FDFD technique has computational advantages compared to EFIE scheme, especially if a non-homogeneous background, like the half-space configuration in GPR, is required in the inversion. Only TM polarization (essentially, 2D problem) has been treated so far with finite difference CSI method. Unfortunately, this method always requires a good initial guess to prevent the iterative inversion process from converging to false local optimal solutions. This problem becomes much more critical in the applications like ground penetrating radar (GPR) and through-wall imaging (TWI), where only one side of the region of interest is available for arranging sensors. To solve this problem, a full polarization inversion method based on FDFD and frequency hopping scheme was proposed, see Sun et al.[7]. This inversion scheme is able to get a good inversion result of buried objects in lossy soil without any a priori information or initial guess of the objects.

In this paper, we applied the above inversion scheme to TWI. The through-wall configuration is incorporated as a priori information in the background configuration of our FDFD inversion scheme. Frequency hopping scheme improves the imaging performance step by step. One advantage of applying the above imaging scheme to TWI is that the permittivity and conductivity of the target behind the wall are always larger than those of the background – the air, therefore the positivity of the contrast can be used as a priori information to further enhance the imaging performance. 2D through-wall simulation is given in section V, and results show that the permittivity and conductivity of the targets behind the wall can be well reconstructed.

II. Problem Statement

Consider the time factor $\exp(j\omega t)$ with $j=\sqrt{-1}$, the electric field equation can be obtained according to [8],

$$\nabla\times\mu^{-1}\nabla\times\boldsymbol{E}-\omega^2\epsilon\boldsymbol{E}=-j\omega\boldsymbol{J}-\nabla\times\mu^{-1}\boldsymbol{M}, \qquad (1)$$

where $\boldsymbol{E}$ and $\boldsymbol{H}$ are the electric and magnetic fields; $\boldsymbol{J}$ and $\boldsymbol{M}$ are the electric and magnetic current source densities; $\epsilon=\varepsilon+\frac{\sigma}{j\omega}$ and μ are the complex dielectric parameter and magnetic permeability. All these quantities are functions of position $\boldsymbol{r}$ and angular frequency ω.

Consider a scattering configuration (see Fig. 1), which consists of a bounded, simply connected, inhomogeneous domain $\mathcal{D}$ located in an inhomogeneous background medium. The domain $\mathcal{D}$ contains an object $\mathcal{B}$, whose location and index of refraction are unknowns. According to Eq. (1), and assuming the magnetic permeability is invariant, i.e. $\mu=\mu_0$, the total electric field E_p and the incident electric field E_p^{inc} satisfy the following Helmholtz equations

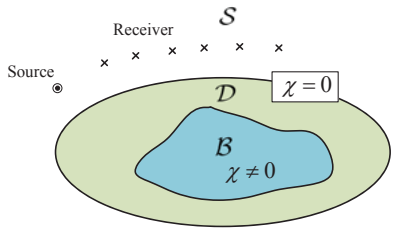

Fig. 1. The scattering configuration in Contrast Source Inversion method.

$$\nabla \times \mu_0^{-1} \nabla \times \boldsymbol{E}_p - \omega^2 \epsilon \boldsymbol{E}_p = -j\omega \boldsymbol{J}_p - \nabla \times \mu_0^{-1} \boldsymbol{M}_p, \quad (2)$$

$$\nabla \times \mu_0^{-1} \nabla \times \boldsymbol{E}_p^{\text{inc}} - \omega^2 \epsilon_{\text{b}} \boldsymbol{E}_p^{\text{inc}} = -j\omega \boldsymbol{J}_p - \nabla \times \mu_0^{-1} \boldsymbol{M}_p, \quad (3)$$

where p represents different sources at different positions. We define the scattered electric field $\boldsymbol{E}_p^{\text{sct}}$ as follows

$$\boldsymbol{E}_p^{\text{sct}} = \boldsymbol{E}_p - \boldsymbol{E}_p^{\text{inc}}. \quad (4)$$

Subtracting Eq. (2) from (3), and using the definition in Eq. (4), we obtain

$$\nabla \times \mu_0^{-1} \nabla \times \boldsymbol{E}_p^{\text{sct}} - \omega^2 \epsilon_{\text{b}} \boldsymbol{E}_p^{\text{sct}} = \omega^2 \chi \boldsymbol{E}_p, \quad (5)$$

in which the contrast χ is given by

$$\chi = \epsilon - \epsilon_{\text{b}} = \varepsilon^{\text{c}} + \sigma^{\text{c}}/(j\omega), \quad (6)$$

where $\varepsilon^{\text{c}} = \varepsilon - \varepsilon_{\text{b}}$ and $\sigma^{\text{c}} = \sigma - \sigma_{\text{b}}$ are the contrast permittivity and the contrast conductivity, respectively. The inverse scattering problem is to solve the contrast χ with incomplete measurement data of the scattered field.

III. FDFD-BASED CSI FORMULATION

Note that Eq. (5) have the same form of (1), which means we could solve $\boldsymbol{E}_p^{\text{sct}}$ with FDFD. Specifically, we have

$$A e_p^{\text{sct}} = \omega^2 \chi e_p, \quad (7)$$

where A is the FDFD stiffness matrix, e_p^{sct} and e_p are the scattered electric field and the total electric field in the form of a column vector. Then we could get the solution of (7) by $e_p^{\text{sct}} = A^{-1} b_p$. Note that if $\boldsymbol{r} \notin \mathcal{B}$, then $\chi = 0$, and if $\boldsymbol{r} \in \mathcal{S}$, then $\boldsymbol{E}_p^{\text{inc}} = \boldsymbol{0}$. Then we obtain the data equations

$$f_p = \mathcal{M}_{\mathcal{S}} A^{-1} \omega^2 \chi e_p, \quad \boldsymbol{r} \in \mathcal{S}, \quad (8)$$

and the state equations

$$e_p = e_p^{\text{inc}} + \mathcal{M}_{\mathcal{D}} A^{-1} \omega^2 \chi e_p, \quad \boldsymbol{r} \in \mathcal{D}, \quad (9)$$

respectively, where $\mathcal{M}_{\mathcal{S}}$ is an operator that interpolates field values defined at the finite-difference grids to the appropriate receiver positions; $\mathcal{M}_{\mathcal{D}}$ is an operator that selects fields only on the object domain $\mathcal{D}$. In our simulation, we could simply assume that the transmitting antennas and receiving antennas are precisely located at the grid positions, so that $\mathcal{M}_{\mathcal{S}}$ and $\mathcal{M}_{\mathcal{D}}$ are matrices with nonzero value "1" only for part of the diagonal elements, which correspond to the positions of antennas and the domain of $\mathcal{D}$, respectively.

Multiply χ at both sides of equations (9), and define the contrast source $J_p = \chi e_p$, we obtain the state equations as follows

$$\chi e_p^{\text{inc}} = J_p - \chi \mathcal{M}_{\mathcal{D}} A^{-1} \omega^2 J_p, \quad \boldsymbol{r} \in \mathcal{D}. \quad (10)$$

Define the data error and the state error as follows

$$\rho(J_p) = f_p - \mathcal{M}_{\mathcal{S}} A^{-1} \omega^2 J_p, \quad (11)$$

$$r(J_p) = \chi e_p - J_p, \quad (12)$$

with

$$e_p = e_p^{\text{inc}} + \mathcal{M}_{\mathcal{D}} A^{-1} \omega^2 J_p. \quad (13)$$

The cost functional is a superposition of the two above errors, and the basic procedure of CSI is that first the contrast source J_p is updated by minimizing the cost functional with an initial guess of the contrast χ_0, then the contrast χ is updated subsequently. A good inversion can be obtained after a number of iterations. More details of the FDFD-based CSI method can be found in [5].

IV. HYBRID POLARIZATION AND FREQUENCY HOPPING INVERSION SCHEME

To deal with TE-polarized excitations based on finite difference scheme, the structure of the Yee's staggered grids requires special treatment. Specifically, each of the three spatial components in the Cartesian coordinates needs to be adjusted to the same position while updating the contrast χ, and the contrast χ also needs to be readjusted backward to the Yee's staggered grids. Accordingly, we define a so-called adjusting operator and readjusting operator, which are represented by $F(\cdot)$ and $\tilde{F}(\cdot)$ respectively. Then in each iteration, the contrast is updated by

$$\chi_n = \frac{\sum_{p,\gamma} F(J_{\gamma,p,n}) \overline{F(e_{\gamma,p,n})}}{\sum_{p,\gamma} \left\| F(e_{\gamma,p,n}) \right\|^2}, \quad (14)$$

where, $\gamma \in \{x, y, z\}$ represents the three coordinates, and $\overline{(\cdot)}$ represents the conjugate operator. $\rho(J_p)$ and $r(J_p)$ are updated subsequently with $\tilde{F}(\chi_n)$.

Here we have a priori information that the real part the contrast is positive, and the imaginary part of the contrast is negative. The positivity constraint can be easily implemented by enforcing the negative value of $\text{Re}(\chi_n)$ and the positive value of $\text{Im}(\chi_n)$ to zero after each update of the contrast. The basic idea of frequency hopping scheme is that a coarse inversion result χ_0 is first obtained by a low frequency f_0, then χ_0 is taken as the initial guess in the next inversion process based on a higher frequency f_1. An important issue is that not only the initial guess of the contrast source J_p needs to be updated, but also the initial guess of the total electric field does. In the following simulations, four frequencies are used to image the objects behind a wall. The basic procedure of the hybrid polarization inversion method based on FDFD and frequency hopping scheme is given in Algorithm 1, in which k is the subscript of the operating frequencies.

V. SIMULATION RESULTS

In our simulation, a 2D through-wall configuration is used which is shown in Fig. 2. The wall is 15 cm thick with the relative permittivity of 5 and the conductivity of 10 mS/m, respectively. Three circular cylinders are located behind the wall, two of which are solid circular cylinders with a 10 cm

Algorithm 1 TE and TM hybrid polarization inversion method based on FDFD and frequency hopping scheme

$J_{p,0} = e_p^{0,\text{inc}}$, $\chi_0 = \mathbf{1}$
Update $e_{p,0}$
for $k = 0$ **to** K **do**
  for $n = 1$ **to** N **do**
    Update χ by $\chi_n = \frac{\sum_{p,\gamma} F(J_{\gamma,p,n})\overline{F(e_{\gamma,p,n})}}{\sum_{p,\gamma}\|F(e_{\gamma,p,n})\|^2}$
    Enforce positivity constraint to χ_n
    Update $\rho_n(J_p)$ and $r_n(J_p)$ with $F(\chi_n)$
    Update $J_{p,n}$
    Update $e_{p,n}$
  end for
  $\chi_0 = \text{Re}(\chi_N) + j\frac{\omega_k}{\omega_{k+1}}\text{Im}(\chi_N)$
  Initialize $e_{p,0}$ and $J_{p,0}$ based on the properly interpolated contrast χ_0
end for
$\varepsilon^{\text{c}} = \text{Re}(\chi_N)$
$\sigma^{\text{c}} = -\text{Im}(\chi_N)\omega_K$

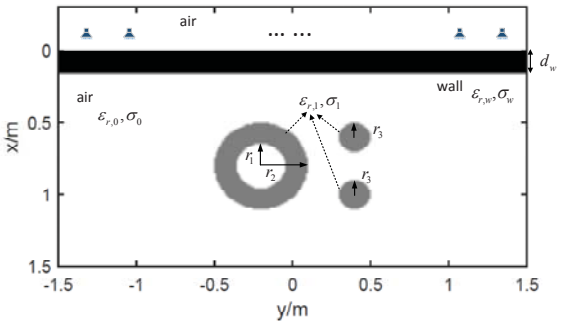

Fig. 2. The through-wall imaging configuration in the simulation

radius, and the left one is hollow with 30 cm outer radius and 15 cm inner radius. See Table I for all the simulation parameters. Three operating frequencies are used, which are $f_1 = 200$ MHz, $f_2 = 300$ MHz, and $f_3 = 400$ MHz, respectively. 15 ideal dipole antennas are arranged uniformly in line with 11 cm away from the surface of the wall. The antennas are able to operate in two modes, TE polarization and TM polarization, respectively. Each time only one antenna transmits the incident wave, and the left antennas collect the measurement data. Synthetic data are generated by a FDFD package which can be downloaded from [9]. The scattered field is obtained by subtracting the incident field from the measurement data. One thing worth noting is that this FDFD package is a 3D Maxwell equation solver. To obtain a 2D configuration, periodic boundary condition is used in the design of the FDFD stiffness matrix.

TE and TM hybrid polarization FD-CSI method is used for inversion. First, we do inversion with 200 MHz. Then, frequency hopping scheme is used to improve the inversion results by taking the outcome of the previous inversion as the initial guess of the current inversion. Positivity constraint is enforced to further enhance the inversion performance. A difference measurement between the newly updated result and

TABLE I. SIMULATION PARAMETERS

Parameter	Value
d_{w}	15 cm
r_1	15 cm
r_2	30 cm
r_3	10 cm
$\varepsilon_{\text{r,0}}$	1
$\varepsilon_{\text{r,w}}$	5
$\varepsilon_{\text{r,1}}$	3
σ_0	0 mS/m
σ_{w}	10 mS/m
σ_1	15 mS/m

the previous result is defined by

$$d_\chi = \frac{\|\chi_n - \chi_{n-1}\|_2}{\|\chi_{n-1}\|_2} \tag{15}$$

The iterative inversion process is terminated if d_χ is less than a certain threshold. In this simulation, the terminating condition is set as $d_\chi < 10^{-3}$.

Fig. 3 shows the reconstructed contrast relative permittivity ε^{c} and contrast conductivity σ^{c} after each frequency hopping. Note that the unit of the contrast conductivity is S/m. The real positions of the three cylinders are depicted with red line. As we can see, the inversion results are improved by increasing the operating frequency based on our frequency hopping scheme. Specifically, the contrast relative permittivity and the contrast conductivity are more and more focused on the real region. The estimated values are underestimated. The reason is that EM waves attenuates in lossy materials. Besides, since the investigating angle is limited, the forward scattering information is totally lost. In addition, we can see that the conductivity is not reconstructed well. The reason is that the real value of the conductivity of the objects are much smaller than that of the relative permittivity. Furthermore, the imaginary part of the contrast χ, RE(χ), gets even smaller as the operating frequency goes high. According to our simulation, we summarize as follows:

1) If RE(χ) $\gg$ Im(χ), then the estimation of the permittivity is more accurate;
2) If RE(χ) $\ll$ Im(χ), then the estimation of the conductivity is more reliable;
3) If RE(χ) and Im(χ) are comparable, then both the permittivity and the conductivity can be well estimated.

For the sake of comparison, Fig. 4 gives the inversion results with single frequency, 300 MHz and 400 MHz, respectively. Although 300 MHz performs very well for inversion, one do not exactly know which is the best frequency for inversion beforehand. In through-wall imaging, the investigation angle is limited. Thus, inversion becomes a seriously ill-posed problem. Single frequency is not enough in most of the cases.

Simulation results show that further increasing the operating frequency does not improve the inversion performance too much. This can be simply explained from the physical aspect. As the operating frequency goes high, the wall and the targets get more and more impenetrable because of serious attenuation of EM wave. In another word, less scattering information is contained in higher frequency measurement data.

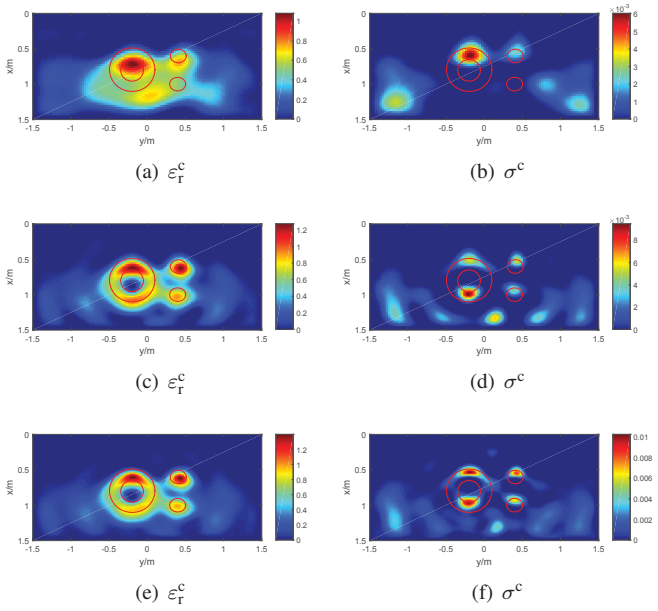

(a) ε_r^c (b) σ^c

(c) ε_r^c (d) σ^c

(e) ε_r^c (f) σ^c

Fig. 3. Inversion results obtained by the TE and TM hybrid polarization CSI method based on FDFD and frequency hopping scheme. (a-b) are inversion results by 200 MHz after 377 iterations; (c-d) are inversion results by 300 MHz with (a-b) as the initial guess after 216 iterations; (e-f) are inversion results by 400 MHz with (c-d) as the initial guess after 56 iterations.

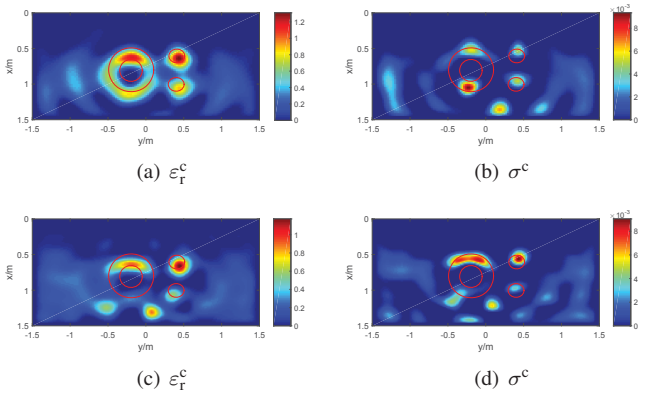

(a) ε_r^c (b) σ^c

(c) ε_r^c (d) σ^c

Fig. 4. Inversion results obtained by the TE and TM hybrid polarization CSI method based on FDFD scheme. (a-b) are inversion results by 300 MHz after 349 iterations; (c-d) are inversion results by 400 MHz after 368 iterations.

VI. Conclusion

In this paper, the TE and TM hybrid polarization CSI method based on FDFD and frequency hopping scheme has been applied to TWI. Positivity constraint is used in the inversion process. 2D through-wall simulation results show that the permittivity and conductivity of the targets behind the wall can be well reconstructed. However, only the dominant component of the contrast χ can be well recovered, and the value is always underestimated. Solving the aforementioned problems requires more efforts, and this is our future work as well.

References

[1] P. M. Van Den Berg and R. E. Kleinman, "A contrast source inversion method," *Inverse problems*, vol. 13, no. 6, p. 1607, 1997.

[2] B. Kooij, M. Lambert, and D. Lesselier, "Nonlinear inversion of a buried object in transverse electric scattering," *Radio Science*, vol. 34, no. 6, pp. 1361–1371, 1999.

[3] T. Isernia, L. Crocco, and M. D'Urso, "New tools and series for forward and inverse scattering problems in lossy media," *Geoscience and Remote Sensing Letters, IEEE*, vol. 1, no. 4, pp. 327–331, 2004.

[4] L. Crocco, M. D'Urso, and T. Isernia, "The contrast source-extended Born model for 2D subsurface scattering problems," *Progress In Electromagnetics Research B*, vol. 17, pp. 343–359, 2009.

[5] A. Abubakar, W. Hu, P. Van Den Berg, and T. Habashy, "A finite-difference contrast source inversion method," *Inverse Problems*, vol. 24, no. 6, p. 065004, 2008.

[6] A. Abubakar, G. Pan, M. Li, L. Zhang, T. Habashy, and P. van den Berg, "Three-dimensional seismic full-waveform inversion using the finite-difference contrast source inversion method," *Geophysical Prospecting*, vol. 59, no. 5, pp. 874–888, 2011.

[7] S. Sun, B. J. Kooij, T. Jin, and A. Yarovoy, "Simultaneous TE and TM polarization inversion based on FDFD and frequency hopping scheme in ground penetrating radar (to be published)," in *Advanced Ground Penetrating Radar (IWAGPR), 2015 8th International Workshop on*. IEEE, 2015, pp. 1—5.

[8] W. Shin, "3D finite-difference frequency-domain method for plasmonics and nanophotonics," Ph.D. dissertation, Stanford University, 2013.

[9] ——. (2015) MaxwellFDFD Webpage. https://github.com/wsshin/maxwellfdfd.